# Process Maps for Controlling Residual Stress and Melt Pool Size in Laser-Based SFF Processes

**Aditad Vasinonta and Jack Beuth**
Department of Mechanical Engineering
Carnegie Mellon University
Pittsburgh, PA

**Michelle Griffith**
Sandia National Laboratories
Albuquerque, NM

## Abstract

Thermal control of solid freeform fabrication processes is critical for obtaining consistent build conditions and in limiting residual stress-induced tolerance losses. In this paper, thermomechanical models are presented for the building of thin-walled structures by laser-based SFF processes. The simulations are used to develop two non-dimensional plots (termed process maps) that quantify the effects of changes in wall height, laser power, deposition speed and part preheating on melt pool size (for consistent build conditions) and thermal gradients (for limiting residual stresses). Mechanical simulations are used to demonstrate the link between thermal gradients and maximum final residual stresses. Models are applied to the Laser Engineered Net Shaping (LENS) process; however, the general approach, insights and conclusions are applicable to most SFF processes involving a moving heat source. The two process maps described herein can be used together to determine optimal process variables for obtaining consistent melt pool length while limiting residual stress in the part. Results from the residual stress simulations also identify two important mechanisms for reducing residual stresses and quantify maximum stress reductions that can be achieved through manipulation of all process variables.

## Nomenclature

| | | | |
|---|---|---|---|
| $T$ | = temperature | $T_m$ | = melting temperature |
| $T_{base}$ | = base plate and wall preheat temperature | $T_{top}$ | = top surface temperature |
| $k$ | = thermal conductivity | $\rho$ | = density |
| $t$ | = wall thickness | $c$ | = specific heat |
| $L$ | = wall length | $h$ | = wall height |
| $Q$ | = laser power | $l$ | = melt pool length |
| $\alpha$ | = fraction of laser power absorbed by the wall | $V$ | = travel speed of laser |

## Introduction

Residual stress-induced tolerance loss is a concern in nearly all solid freeform fabrication (SFF) processes. This includes processes based on successive curing of polymers as well as those based on successive thermal deposition of polymers or metals. In using SFF processes for rapid prototyping, some tolerance loss due to residual stresses is generally acceptable; however, many targeted applications for using SFF processes as rapid manufacturing techniques (to create functional parts) have strict dimensional limits. Residual stress-induced deformation is also becoming a greater concern as SFF processes are used to build large parts, where larger part dimensions naturally lead to larger dimensional losses.

A critical issue in developing SFF processes as rapid manufacturing techniques is the alteration of the processes to control residual stresses while maintaining optimal deposition conditions. In this research, two non-dimensional plots (termed process maps) are presented, which

are developed from numerical models of laser-based material deposition of thin-walled structures. These process maps show the effects of changes in laser power, deposition speed, part preheating and wall height on two process parameters. They are melt pool length, which has been identified as a critical parameter for maintaining optimal build conditions, and a defined temperature gradient, which can be linked to the final maximum stress in the part.

The principal application of this work is to the Laser Engineered Net Shaping (LENS) process under development at Sandia National Laboratories [1]. In the LENS process, parts are constructed by focusing a high-power laser beam onto a metal substrate, where streams of metallic powder are simultaneously injected. The laser locally melts the powder to form a molten pool on the top surface of the growing part. By moving the laser beam, parts are built up, line by line and layer by layer. Work is underway at Sandia Labs to not only optimize process parameters manually, but to use real-time thermal images of melt pool size as a feedback mechanism to control the process [2]. Process maps presented in this paper have been developed to aid in both manual and automated process control efforts. Although this research is directed toward the LENS process, the approach taken is applicable to any solid freeform fabrication process involving a moving heat source, and many of the conclusions are relevant to all SFF processes involving thermal deposition of metals.

**Geometry Considered, Numerical Model and Non-Dimensional Variables**

*Geometry Considered:* In the current study, the thin-walled structure shown in Fig. 1 is considered. Thin-walled geometries of this type are commonly fabricated using the LENS and other SFF processes. Also, numerical simulations of a wall of large height, $h$, with temperature-independent properties can be verified against an existing analytical solution in the literature [3]. It is assumed that the thin wall is fabricated by depositing material along a single row; thus, the thickness of the wall is comparable to the molten melt pool size. The distance traveled by the laser and the length of the wall in the x direction are assumed large enough that steady-state conditions exist independent of the existence of the vertical free surfaces. It is assumed that the wall is built upon a large metallic substrate, which acts as a thermal heat sink and mechanically constrains the wall from deformation during the manufacturing process. Results presented herein demonstrate how melt pool length (extent in the x-direction) and final maximum residual stress can be controlled as a function of wall height, $h$, absorbed laser power, $\alpha Q$, laser velocity in the x-direction, $V$, and uniform preheating of the wall and base plate to a temperature $T = T_{base}$.

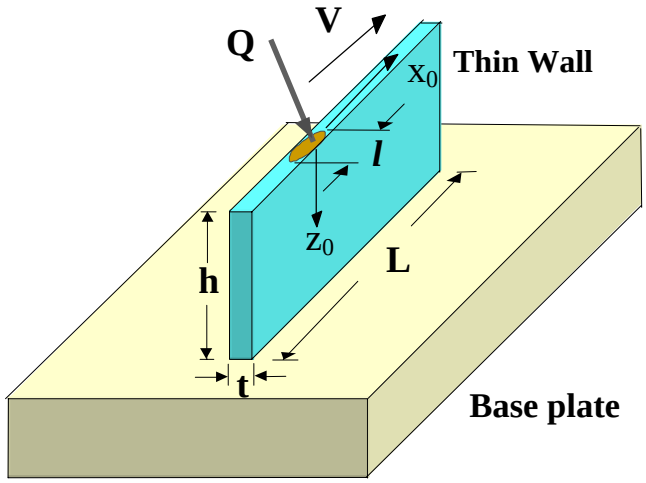


Figure 1. Thin-Walled Geometry Considered in This Study

*Numerical Model:* The strategy for solving problems of thermally induced residual stress is to first obtain a thermal solution, then use its temperature predictions as inputs to a mechanical model. The thermal models used in this study do not include the effects of convective heat transfer from the wall free surfaces to the surrounding air and do not model convective flows in the melt pool itself. Work by Dobranich and Dykhuizen [4] suggests strongly that the role of these effects in determining melt pool size is not significant. The models of this study also model the laser as a point source of heat, neglecting the distribution of laser power over the melt pool region. Assuming a point source of power is reasonable given the goal of this study, which is to capture changes in melt pool size, temperature gradient and other parameters as a function of changes in the process variables outlined above. Accuracy in the absolute predictions is of secondary importance. It is shown later in this paper, however, that model predictions for melt pool length still compare reasonably well with experimentally determined melt pool sizes.

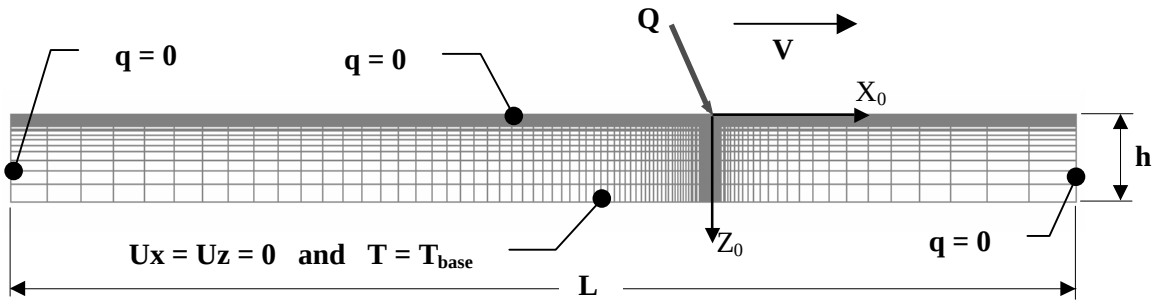


Figure 2. 2-D Thermomechanical Model and Boundary Conditions

The mesh and boundary conditions used for a typical 2-D thermomechanical model of this study are shown in Fig. 2. In each set of simulations, the meshes used in both thermal and mechanical models are identical. Four-noded bilinear elements are used as part of the ABAQUS finite element software package. The laser beam focused on the top surface of the substrate is simulated by a point source of power subsequently applied at model nodes at a rate simulating the laser velocity. Because of high temperature and displacement gradients in the region near heat source, the grid is biased toward the region that will surround the heat source at the time when results are to be extracted from the model. In addition to comparisons of the thermal model with an analytical solution valid for a large substrate [3], the convergence of this mesh was checked against thermal and mechanical models with roughly half the resolution in the x and z directions with no noticeable change in the results.

As illustrated in Fig. 2, in the thermal simulations an insulated boundary condition is imposed on the top and both vertical sides of the substrate. The temperature along the substrate bottom is specified as fixed at a value equal to the temperature of the base plate. Sensitivity studies have shown that specifying boundary conditions along the substrate vertical and top surfaces as being insulated or convective has little effect on thermal results near the heat source. Most of the heat transferred from the laser is conducted out through the bottom of the substrate. By using a 2-D model, it is also assumed that there is no heat loss through the front and back surfaces of the wall. In the mechanical simulations, vertical and horizontal displacements are prohibited along the bottom of substrate. The remaining boundaries are modeled as traction free.

Thermal and mechanical properties of AISI 304 stainless steel (SS304), which is used in the LENS and other SFF metal deposition processes, are used as inputs for the thermal and stress simulations respectively. Thermal properties were taken from [4] whereas the mechanical properties were taken from [5]. These properties are comparable to those used by Klingbeil, et al. [6] in thermomechanical modeling of the Shape Deposition Manufacturing (SDM) process. The

properties used in the model that are set to depend on temperature are density, specific heat, thermal conductivity, Young's modulus, thermal expansion coefficient and yield stress. The latent heat of the liquid-solid phase transition is also included in the model. Creep is not included in the constitutive modeling; however, thermomechanical modeling of the SDM process by Chin [7] indicates that it is not needed to accurately predict room temperature stresses for SS304. At present, the authors are investigating the effect of strain hardening; therefore, it is not yet included in the results presented in this paper.

*Non-Dimensional Variables:* A 2-D conductive heat transfer solution for a point heat source moving across a semi-infinite substrate was first developed by Rosenthal [3]. The temperature solution and its derivative with respect to $Z_0$ can be expressed in terms of modified Bessel functions of second kind (K). Insightful studies of application of this 2-D solution to the LENS process are given in [8] and [9]. As suggested by the Rosenthal solution, the normalization for melt pool length for the problem of Fig. 1 can be represented through three dimensionless variables: the normalized melt pool length ($\bar{l}$), normalized height of substrate ($\bar{h}$) and the normalized melting temperature ($\bar{T}_m$). They are defined as follows:

$$\bar{l} = \frac{l}{2k/\rho cV}, \qquad \bar{h} = \frac{h}{2k/\rho cV} \qquad \text{and} \qquad \bar{T}_m = \frac{T_m - T_{base}}{\alpha Q/\pi kt}. \tag{1}$$

This normalization scheme is chosen so that results for normalized melt pool length, $\bar{l}$, are presented as a function of normalized wall height, $\bar{h}$, and normalized melting temperature, $\bar{T}_m$.

The temperature gradient (in the $Z_0$ direction) can also be normalized and represented by dimensionless variables. At any fixed normalized depth, $\bar{Z}_0$, the normalized temperature gradient, $\frac{\partial \bar{T}}{\partial \bar{Z}_0}$, can be presented as a function of normalized wall height, $\bar{h}$, and normalized top surface temperature ($\bar{T}_{top}$). The dimensionless variables for the normalization of temperature gradient are

$$\frac{\partial \bar{T}}{\partial \bar{Z}_0}, \qquad \bar{T}_{top} = \frac{T_{top} - T_{base}}{\alpha Q/\pi kt}, \qquad \bar{h} = \frac{h}{2k/\rho cV} \qquad \text{and} \qquad \bar{Z}_0 = \frac{Z_0}{2k/\rho cV}. \tag{2}$$

In fixing the $X_0$ location of the thermal gradient, the dimensionless variable $\bar{T}_{top}$ has been chosen instead of $\bar{X}_0$. This is because it is more physically relevant to use the temperature on the top surface as one of the criteria for specifying the location for extracting the temperature gradient. These criteria are discussed later in this paper.

**Results for Melt Pool Length**

A process map for melt pool length for a thin-walled structure with a concentrated laser heat source moving across it has been developed and reported in [10] and [11]. The work described in [10] uses slightly different normalization rules than are used in [11] and herein. The process map is shown in Fig. 3, which consists of three surfaces plotted on three coordinate axes. The middle surface was developed from several numerical simulations with temperature-independent properties performed with differing wall heights in order to get the dependence of $\bar{l}$ on $\bar{h}$. The dependence of $\bar{l}$ on $\bar{T}_m$ was then determined from the same simulations by assuming different values of $T_m$. The results from temperature-dependent simulations are also presented in Fig. 3 as the upper and lower error surfaces that bound the temperature-independent results. The space between these error

surfaces reflects the range in results seen when process variables are varied over the range of specific interest in the LENS process. That range consists of values of $\alpha Q$ from 43.2 to 165 W, $V$ from 5.93 to 9.31 mm/sec and $T_{base}$ from 30° C to 400° C. The detailed assumptions and procedures for obtaining and using the process map for melt pool length are given in [11]. In brief, the process map of Fig. 3 can be used effectively for SS304 deposition within the range of process parameters of interest in the LENS process by applying the following four rules:

1. Properties at 1000 K are used in the normalization;
2. For cases involving a change in preheat, a linear change in thermal conductivity with a preheat temperature is assumed, as given in the following equation,
$$k = 24.3 + 0.013(T_{base} - 30) \qquad W/(mK). \qquad (3)$$
3. For predicting steady-state melt pool lengths due to a change in process variables, wall thickness is assumed to scale proportionally with melt pool length; and
4. It is assumed that the melt pool length/wall thickness scaling is unaffected by velocity.

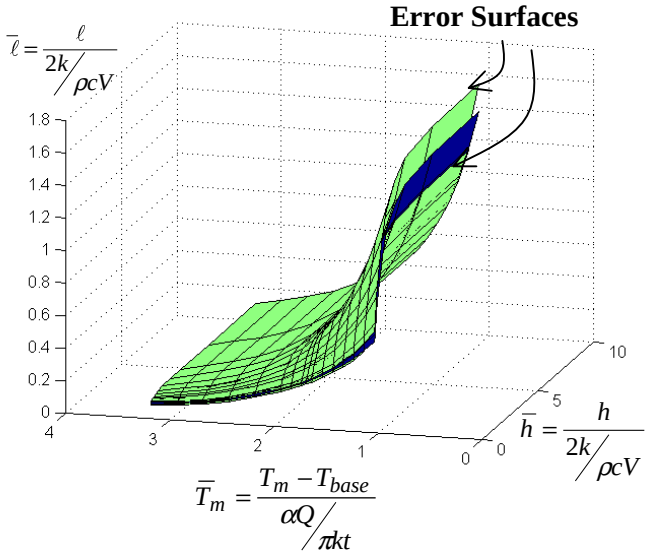


Figure 3. Process Map for Melt Pool Length.

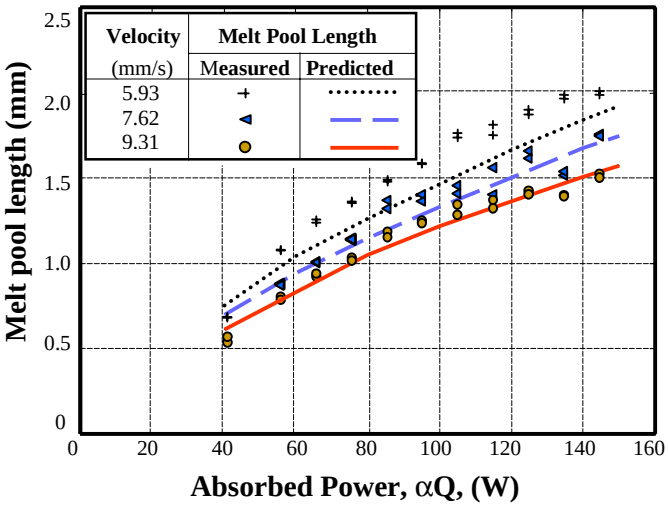


Figure 4. Comparison of Predicted and Measured Melt Pool Lengths

It can be seen from Fig. 3 that at each fixed $\bar{h}$, $\bar{l}$ increases with increasing $T_{base}$ or $Q$ (either of which decreases $\bar{T}_m$). Moreover, a change in $T_{base}$ can be compensated for by a change in Q, to retain a desired melt pool length. When the wall is relatively tall, $\bar{h}$ has no significant effect on $\bar{l}$, because the wall is tall enough that the effect of the fixed temperature at the base is not seen at the melt pool. In contrast, $\bar{h}$ has a considerable effect on melt pool length when the wall is relatively short, with $\bar{l}$ dropping rapidly as $\bar{h}$ is reduced. Melt pool size can also be changed through a change in laser velocity, V. This is most easily seen for large values of $\bar{h}$ (so that its dependence on $V$ does not change $\bar{l}$). Through the normalization scheme used, the actual melt pool length, $l$, is given by:

$$l = \frac{2k\bar{l}}{\rho cV} \quad . \qquad (4)$$

Thus, for a fixed value of $\bar{l}$ as determined from the process map, $l$, is increased by a decrease in V.

Figure 4 provides a comparison of measured melt pool lengths as a function of laser power and velocity to predictions provided by the process map of Fig. 3 using the rules outlined above.

The only inputs used to generate the predictions from the process map were a single experimentally measured wall thickness of t = 1.3 mm for ambient conditions of $V$ = 7.62 mm/sec and $\alpha Q$ = 105 W (based on an assumed value of $\alpha$ = 0.35 as suggested by Dobranich and Dykhuizen [4]). Measurements were made using real-time thermal imaging methods described briefly in [2]. The experimental results presented are for a single set of observations [12] and do not reflect the variability seen in measured results at nominally identical conditions, which can easily be on the order of $\pm 5\%$. Because $\alpha$ is not known precisely, caution is suggested in directly comparing measured and predicted values in Fig. 4. However, the predictions of the process map are clearly capturing the trends in the measured results, which is the goal of this research.

**Results for Temperature Gradient**

The thermomechanical models used in this study are designed to capture residual stress magnitudes and to demonstrate their link to defined temperature gradients. Theoretically, the second derivative of temperature is the key parameter that controls residual stress. A linear temperature field produces identically zero stress throughout a body, provided that all external restraints are absent [13]. However, for the thin-walled problem considered herein, the temperature gradient near the top of the wall is directly related to the second derivative of temperature in that region. Since the temperature gradient at the top surface is zero, a temperature gradient extracted from the top portion of the model scales with the average change in gradient between that point and the top surface. By using the process map of temperature gradient presented herein, one can extract the representative normalized temperature gradient for a thin wall for any known values of process variables. This normalized temperature gradient can then easily be converted to the actual temperature gradient, which is the parameter linked to the maximum final residual stress.

Two rules have been established to specify the location for extracting a representative temperature gradient for a thin-walled structure. First, the temperature gradient is extracted at a normalized depth ($\overline{Z}_0$) equal to 1.2. This normalized depth has been chosen because it gives the maximum value of temperature gradient for typical process parameters for the LENS process. For different sets of process parameters, the maximum temperature gradient will occur at different normalized depths. However, within the range of process variables considered, the variation of this depth is small. By fixing the normalized depth, the temperature gradient is simplified to a function of normalized height of the wall ($\overline{h}$) and normalized temperature at top surface ($\overline{T}_{top}$). The second rule established by the authors is to extract the temperature gradient at a location behind the heat source where the temperature on the top surface is 1150 K. The temperature of 1150 K was chosen based on results from Chin [7] regarding residual stresses for the SDM process. That work suggests that, for SS304, a substantial amount of stress build-up occurs at temperatures below 1150 K. Residual stress magnitudes are relatively small at temperatures higher than 1150 K. In addition, a plot of yield stress vs. temperature for SS304 shows that when the temperature drops below 1150 K, the yield stress increases significantly. These facts suggest that the temperature gradients (and their derivatives) near 1150 K establish the strain mismatches that the thin wall is subjected to, as it cools, in the temperature range where the yield stress is significantly large. It is therefore likely that they are important in determining magnitudes of the final residual stresses.

Using the normalization scheme of eq. [2], the process map for temperature gradient at a normalized depth $\overline{Z}_0$ = 1.2 has been developed and is shown in Fig 5. Analogous to the process map for the melt pool length, the process map for temperature gradient presents the dependence of the normalized temperature gradient, $\left.\frac{\partial \overline{T}}{\partial \overline{Z}_0}\right|_{\overline{Z}_0=1.2}$, on normalized height ($\overline{h}$) and dimensionless

temperature ($\overline{T}_{Top}$). The process map was developed from several simulations using temperature-independent material properties. Efforts are currently underway to develop a process map for temperature gradient that includes temperature-dependent properties.

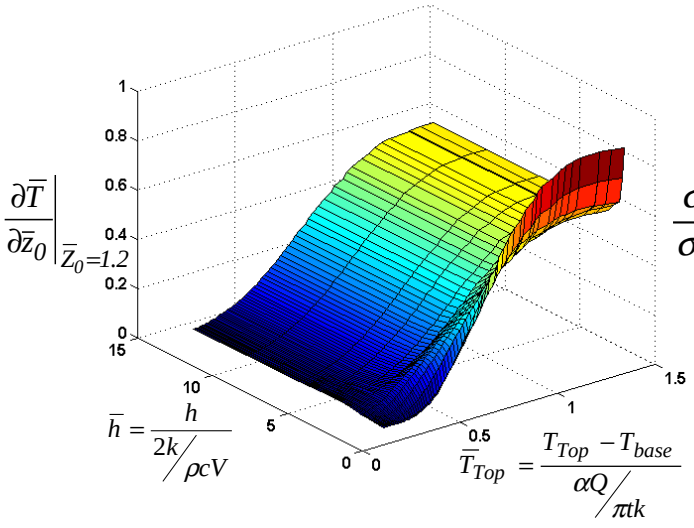


Figure 5. Process Map for Temperature Gradient

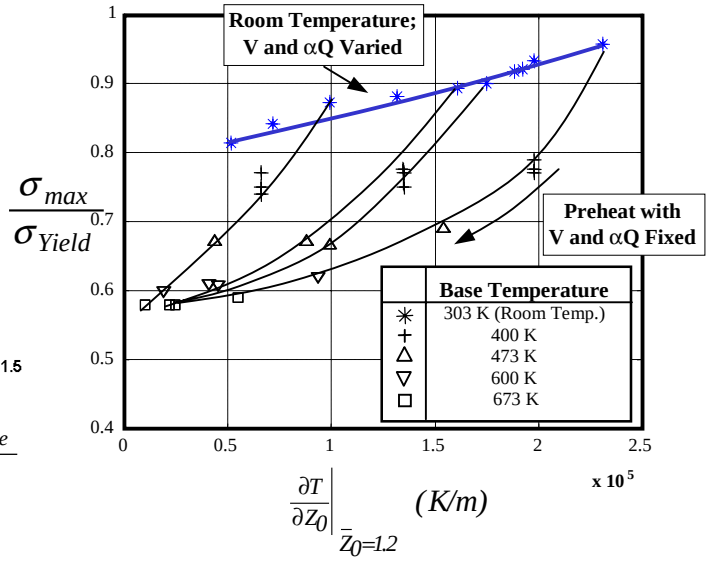


Figure 6. Relation of Maximum Final Stresses to Temperature Gradient

It can be seen from Fig. 5 that, as in the case of melt pool length, $\overline{h}$ has a considerable effect on the normalized temperature gradient when the wall is relatively short. Due to the large difference between $T_{base}$ and $T_{top}$, $\left.\frac{\partial \overline{T}}{\partial \overline{Z}_0}\right|_{\overline{Z}_0=1.2}$ near the heat source increases rapidly as $\overline{h}$ is reduced. At each fixed $\overline{h}$, the normalized temperature gradient decreases with decreasing $\overline{T}_{top}$ (as one moves away from the heat source). If $T_{top}$ is fixed at 1150 K, $\left.\frac{\partial \overline{T}}{\partial \overline{Z}_0}\right|_{\overline{Z}_0=1.2}$ decreases with increasing $T_{base}$ or Q. The normalized temperature gradient can also be decreased through a decrease in velocity, V. This is most easily seen for large values of $\overline{h}$ (so that its dependence on $V$ does not change $\left.\frac{\partial \overline{T}}{\partial \overline{Z}_0}\right|_{\overline{Z}_0=1.2}$). Through the normalization scheme used, the actual temperature gradient is given by:

$$\left.\frac{\partial T}{\partial Z_0}\right|_{\overline{Z}_0=1.2} = \frac{\rho c V \alpha Q}{2\pi k^2 t} \left.\frac{\partial \overline{T}}{\partial \overline{Z}_0}\right|_{\overline{Z}_0=1.2} \qquad (5)$$

Thus, for a fixed normalized temperature gradient, $\left.\frac{\partial T}{\partial \overline{Z}_0}\right|_{\overline{Z}_0=1.2}$ is decreased by a decrease in V.

Figure 6 gives results for $\sigma_{max}/\sigma_{yield}$ as a function of actual temperature gradient from thermomechanical simulations of a tall wall using five different values of $T_{base}$. A range of laser power and velocities is also represented, but the plot does not include values that result in large thermal gradients. For these cases deposition onto a room temperature substrate results in maximum stress values equal to $\sigma_{Yield}$. The plot clearly shows the dependence of residual stress on temperature gradient. For results generated using a base plate temperature of 400 K, it is seen that different sets of process parameters produce approximately the same maximum stresses in the part if the representative temperature gradients are matched. Also, as expected, at a fixed base

temperature, the residual stresses decrease with decreasing temperature gradient. This reduction can be explained as being due to a decrease in strain mismatches during cooling. As seen in the plot, the maximum reduction in stress magnitude from the decrease of strain mismatches occurs at room temperature. The line at the top of the plot designating room temperature results includes values of $\sigma_{max}/\sigma_{yield}$ as low as 0.80, so that the maximum reduction in stress (from $\sigma_{Yield}$) achievable by this mechanism is approximately 20%.

By comparing the numerical results at different base temperatures, it is clear that uniform part preheating considerably reduces the residual stress. Some reduction of residual stress is due to reductions in strain mismatch, but most of the reductions due to preheating come from reducing the effective yield stress. The yield stress of SS304 decreases as the temperature increases. By preheating the part, the maximum residual stress is limited by the maximum yield stress. The maximum reduction of residual stress by preheating the part is approximately 40% and is achieved by preheating the part to 400°C.

Thus, in addition to establishing a link between the thermal gradient defined in this study and maximum residual stresses and quantifying the magnitudes of potential residual stress reductions, the plot of Fig. 4 identifies two mechanisms behind the reduction of residual stress. The first mechanism is the decrease of strain mismatches during cooling as the temperature gradient is decreased. This result can be achieved by adjusting laser power and velocity. The second mechanism is the reduction of the effective yield stress, which, in turn, reduces the final maximum residual stress in the part. The reduction of residual stress seen by part preheating mostly comes from this second mechanism.

**Summary and Implications of the Results**

In this study, two process maps have been presented for the building of stainless steel thin-walled structures by laser-based SFF processes. The first process map (which is detailed in [11]) is for predicting or controlling melt pool size, whereas the second process map is for predicting a normalized temperature gradient, which is linked to maximum residual stress magnitudes. While the temperature-dependent results presented in this study are specifically applied to deposition of SS304 via the LENS process, temperature-independent results and insights from them are applicable to any SFF process that involves a moving heat source.

Although they are not presented in detail herein, calculations performed with the process maps described in this study have several major implications relevant to the LENS process and other similar SFF processes. First, a considerable change in melt pool length is predicted to occur for very short walls. Furthermore, because base plate preheating has a minimal effect on melt pool size, it does not appear that this change can be compensated for by a base plate preheat alone. To obtain an optimal melt pool length for short walls, a change in laser power or laser velocity is needed. Residual stress results indicate that for deposition onto a room temperature substrate, changing laser velocity and power can reduce residual stresses by as much as 20% from the yield stress. However, changes in velocity and power will result in significant changes in melt pool size. Furthermore, if preheating is pursued, the pay-off achieved in changing laser power and velocity to decrease thermal gradients is reduced.

The biggest pay-off in reducing residual stresses comes from uniform base plate preheating. The reduction in residual stress that can result from a preheat to 400°C is approximately 40% (from the yield stress). At large levels of base plate preheating, the reduction in residual stress is a very weak function of laser velocity and power. Thus at large levels of preheat, the full range of power and velocity can be used with minimal effects on maximum residual stress magnitudes. Finally,

since preheating does not increase melt pool lengths significantly, any increase in melt pool size due to preheating can easily be eliminated by a small decrease in laser power or increase in laser velocity. In this way, the process maps for melt pool length and temperature gradient presented herein can be used together to suggest strategies for controlling residual stress magnitudes while still maintaining an optimal melt pool length.

**Acknowledgements**

This research has been supported by the National Science Foundation under grant DMI-9700320 and by Sandia National Laboratories under grant BE-0792. The authors would like to thank William Hofmeister and Melissa Wert of Vanderbilt University for providing data from their thermal imaging experiments that has proven to be vital for this research. The authors would also like to thank Emanuel Sachs for his insightful questions and suggestions regarding this research.

**References**

1. Griffith, M.L., Keicher, D.M., Atwood, C.L., Romero, J.A., Smugeresky, J.E., Harwell, L.D. and Greene, D.L., "Freeform Fabrication of Metallic Components Using Laser Engineered Net Shaping (LENS)," *Solid Freeform Fabrication Proceedings*, D.L. Bourell, J.J. Beaman, H.L. Marcus, R.H. Crawford and J.W. Barlow, eds., The University of Texas at Austin, August 1996, pp. 125-132.
2. Griffith, M.L., Schlienger, M.E., Harwell, L.D., Oliver, M.S., Baldwin, M.D., Ensz, M.T., Smugeresky, J.E., Essien, M., Brooks, J., Robino, C.V., Hofmeister, W.H., Wert, M.J. and Nelson, D.V., "Understanding Thermal Behavior in the LENS Process," *Journal of Materials Design*, Vol. 20, No. 2/3, 1999, pp. 107-114.
3. Rosenthal, D., "The Theory of Moving Sources of Heat and Its Application to Metal Treatments," *Transactions of ASME*, Vol. 68, 1946, pp. 849-866.
4. Dobranich, D. and Dykhuizen, R.C., "Scoping Thermal Calculation of the LENS Process," Sandia National Laboratories Internal Report, 1998.
5. Peckner, D. and Bernstein, I.M., *Handbook of Stainless Steels*, McGraw-Hill, 1977, pp. 19-3, 19-7, 21-5 and 21-6.
6. Klingbeil, N.W., Beuth, J.L., Chin, R.K. and Amon, C.H., "Measurement and Modeling of Residual Stress-Induced Warping in Direct Metal Deposition Processes," *Solid Freeform Fabrication Proceedings*, H.L. Marcus, J.J. Beaman, D.L. Bourell, J.W. Barlow and R.H. Crawford, eds., The University of Texas at Austin, August 1998, pp. 367-374.
7. Chin, R.K., "Thermomechanical Modeling of Residual Stresses in Layered Manufacturing with Metals," Ph.D. Thesis, Carnegie Mellon University, May 1998.
8. Dykhuizen, R.C. and Dobranich, D., "Cooling Rates in the LENS Process," Sandia National Laboratories Internal Report, 1998.
9. Dykhuizen, R.C. and Dobranich, D., "Analytical Thermal Models for the LENS Process," Sandia National Laboratories Internal Report, 1998.
10. Vasinonta, A., Beuth, J.L. and Griffith, M., "Process Maps for Laser Deposition of Thin-Walled Structures," *Solid Freeform Fabrication Proceedings*, D.L. Bourell, J.J. Beaman, R.H. Crawford, H.L. Marcus and J.W. Barlow, eds., The University of Texas at Austin, August 1999, pp. 383-391.
11. Vasinonta, A., Beuth, J.L. and Griffith, M., "A Process Map for Consistent Build Conditions in the Solid Freeform Fabrication of Thin-Walled Structures," *Journal of Manufacturing Science and Engineering*, submitted.
12. Hofmeister, W.M. and Wert, M.J., personal communication.
13. Boley, B.A and Weiner, J.H., *Theory of Thermal Stresses*, John Wiley & Sons, Inc., 1960.